24. Schindowski K, Belarbi K, Buee L. Neurotrophic factors in Alzheimer's disease: role of axonal transport. *Genes Brain Behav* 2008; **7** (Suppl 1): 43–56.
25. Howells DW, Porritt MJ, Wong JY *et al.* Reduced BDNF mRNA expression in the Parkinson's disease substantia nigra. *Exp Neurol* 2000; **166**: 127–135.
26. Ishikawa K, Watanabe M, Yoshizawa K *et al.* Clinical, neuropathological, and molecular study in two families with spinocerebellar ataxia type 6 (SCA6). *J Neurol Neurosurg Psychiatry* 1999; **67**: 86–89.
27. Matsuda N, Lu H, Fukata Y *et al.* Differential activity-dependent secretion of brain-derived neurotrophic factor from axon and dendrite. *J Neurosci* 2009; **29**: 14185–14198.
28. Kawamoto Y, Nakamura S, Nakano S, Oka N, Akiguchi I, Kimura J. Immunohistochemical localization of brain-derived neurotrophic factor in adult rat brain. *Neuroscience* 1996; **74**: 1209–1226.
29. Kawamoto Y, Nakamura S, Kawamata T, Akiguchi I, Kimura J. Cellular localization of brain-derived neurotrophic factor-like immunoreactivity in adult monkey brain. *Brain Res* 1999; **821**: 341–349.
30. Murer MG, Boissiere F, Yan Q *et al.* An immunohistochemical study of the distribution of brain-derived neurotrophic factor in the adult human brain, with particular reference to Alzheimer's disease. *Neuroscience* 1999; **88**: 1015–1032.
31. Adachi N, Kohara K, Tsumoto T. Difference in trafficking of brain-derived neurotrophic factor between axons and dendrites of cortical neurons, revealed by live-cell imaging. *BMC Neurosci* 2005; **6**: 42.
32. Kuczewski N, Porcher C, Lessmann V, Medina I, Gaiarsa JL. Activity-dependent dendritic release of BDNF and biological consequences. *Mol Neurobiol* 2009; **39**: 37–49.

Neurobiology of Aging 34 (2013) 1101–1104

Contents lists available at SciVerse ScienceDirect

Neurobiology of Aging

journal homepage: www.elsevier.com/locate/neuaging

Brief communication

Suspected limited efficacy of γ-secretase modulators

Nobuto Kakuda [a,b], Kohei Akazawa [c], Hiroyuki Hatsuta [d], Shigeo Murayama [d], Yasuo Ihara [a,b,e,f,*], The Japanese Alzheimer's Disease Neuroimaging Initiative

[a] Department of Neuropathology, Faculty of Life and Medical Sciences, Doshisha University, Kyoto, Japan
[b] Core Research for Evolutional Science and Technology (CREST), Japan Science and Technology Agency, Saitama, Japan
[c] Department of Medical Informatics, Niigata University Medical and Dental Hospital, Niigata University, Niigata, Japan
[d] Department of Neuropathology, Tokyo Metropolitan Institute of Gerontology, Tokyo, Japan
[e] Center for Neurologic Diseases, Doshisha University, Kyoto, Japan
[f] New Energy and Industrial Technology Development Organization (NEDO), Kanagawa, Japan

ARTICLE INFO

Article history:
Received 16 June 2012
Accepted 25 August 2012
Available online 9 October 2012

Keywords:
γ-Secretase
γ-Modulator
Alzheimer's disease

ABSTRACT

Mild cognitive impairment and Alzheimer's disease (AD) are associated with changes in γ-secretase activity in the brain, producing an amyloid β-protein-42-lowering γ-modulator-like effect. We show here that this modulation occurs at the stage of amyloid deposition, presumably decades earlier than the onset of AD. In addition, γ-secretase modulator-1, a γ-modulator, altered γ-secretase activity in the AD brain but to a lesser extent than in the normal brain. These findings suggest that γ-modulators have limited efficacy against amyloid deposition and AD.

1. Introduction

Amyloid β-protein (Aβ) is cleaved sequentially from amyloid precursor protein by β- and γ-secretases (for a review see Selkoe, 2001). The longer but minor species, Aβ42, predominates in senile plaques (Iwatsubo et al., 1994). γ-Secretase, a heterogeneous complex (Takasugi et al., 2003; Serneels et al., 2009), governs the intramembrane proteolysis of type I membrane proteins including amyloid precursor protein (Sisodia and St George-Hyslop, 2002; Wakabayashi and De Strooper, 2008). We found recently that γ-secretase activity is altered in brains affected by mild cognitive impairment (MCI) or Alzheimer's disease (AD). The change decreases the concentrations of both Aβ42 and Aβ43 in cerebrospinal fluid (CSF) in patients affected with MCI or AD. To compensate for these decreases, the levels of Aβ38 and Aβ40 are increased (Kakuda et al., 2012). We assume that Aβ42 and Aβ43 are enhanced to be converted by stepwise processing to Aβ38 and Aβ40, respectively, by altered γ-secretase in the brain affected by MCI or AD (Kakuda et al., 2012; Takami et al., 2009). Reciprocal changes in the levels of Aβ42 and Aβ38 without a change in the total Aβ level are an essential characteristic of γ-secretase modulators, drugs whose development receives intense attention.

2. Materials and methods

2.1. Subjects

Human cortical specimens for quantification of raft-associated γ-secretase activity were obtained from brains that had been removed, processed, and stored at −80 °C within 12 hours postmortem; the bodies had been placed in a cold (4 °C) room within 2 hours after death. The specimens were kept at the Brain Bank at Tokyo Metropolitan Institute of Gerontology. For all the brains registered at the bank we obtained written informed consent for their use for medical research from the patient or the patient's family. Each brain specimen (approximately 0.5 g) was taken from Brodmann areas 9–11 of 13 AD patients (80 ± 5.0 years of age; Braak neurofibrillary tangle [NFT] stage >IV; senile plaque [SP] stage = C; retrospective clinical dementia rating [CDR] >1), 10 SP stage B patients (76 ± 4.0 years of age; Braak NFT stage >I; retrospective CDR = 0), 10 SP stage A patients (76 ± 4.7 years of age; Braak NFT stage >0; retrospective CDR = 0), and 16 controls in SP stage 0 (77 ± 6.5 years of age; Braak NFT stage <I; retrospective CDR = 0). SP stages were determined by modified methenamine silver stain: stage A: Aβ deposits in the basal portions of the isocortex; stage B: Aβ deposits in virtually all isocortical association

* Corresponding author at: Department of Neuropathology, Faculty of Life and Medical Sciences, Doshisha University, 4-1-1, Kizugawadai, Kizugawa, Kyoto 619-0225, Japan. Tel.: +81 774 65 6058; fax: +81 3 5800 6852.
E-mail address: yihara@mail.doshisha.ac.jp (Y. Ihara).

0197-4580/$ – see front matter © 2013 Elsevier Inc. All rights reserved.
http://dx.doi.org/10.1016/j.neurobiolaging.2012.08.017

areas except primary centers; stage C (AD): Aβ deposits in all areas of the isocortex including primary motor and sensory centers (Braak and Braak, 1991).

2.2. Quantification of brain raft-associated γ-secretase activity

A previously reported assay method was employed with some modifications (Kakuda et al., 2012). Briefly, each raft fraction, adjusted to 100 μg/mL in protein concentration, was incubated with 200 nM of βCTF-FLAG for 1 hour at 37 °C in the presence of 0, or 0.1–0.5 μM γ-secretase modulator (GSM)-1 (kindly provided by Dr M. Okochi, Osaka University). After incubation, all samples were centrifuged at 265,000*g* on a TLA110 rotor (Beckman, Palo Alto, CA, USA) for 20 minutes at 4 °C. The supernatants were separated on sodium dodecyl sulfate polyacylamide gel electrophoresis (SDS-PAGE), and subjected to quantitative Western blot analysis, using specific antibodies, 3B1 for Aβ38, BA27 for Aβ40, 44A3 for Aβ42, and anti-Aβ43 polyclonal for Aβ43.

2.3. GSM-1-induced shift of ln(Aβ38/42)

Shifts of ln(Aβ38/42) with GSM-1 were calculated as GSM-1-induced ln(Aβ38/42) minus the ratio measured in its absence.

2.4. Statistical analysis

All statistical analyses were performed using SPSS version 14.0. Data transformation was required to achieve normal distributions; all analyses were performed after logarithmic transformation of the data for Aβ38, Aβ40, Aβ42, and Aβ43. Analysis of variance was used to test the equality of mean values for continuous variables between the 4 groups: control, SP stage A, SP stage B, and AD. Multiple comparisons were made using Bonferroni *t* test to test the differences between controls, SP stage A, SP stage B, and AD. The paired *t* test was used to examine the effect of GSM-1 treatment. *p* values <0.05 were considered significant.

3. Results

We speculated that this modulation in the γ-secretase activity occurs much earlier than the onset of AD because lower Aβ42 concentrations in CSF appear to be associated with amyloid deposition itself (Fagan et al., 2006). To confirm this, we measured the activities of raft-associated γ-secretase prepared from autopsied brains using a previously established method (Kakuda et al., 2012). Raft fractions were prepared from control and AD brains (Brodmann areas 9–11), which were judged histochemically to be in the Braak SP stage 0, stage A, stage B, or stage C (AD) (Braak and Braak, 1991). Aβs produced by γ-secretase from each brain specimen were analyzed by quantitative Western blot, and the ln(Aβ40/43) and ln(Aβ38/42) ratios were obtained. Stage A plots nearly superimposed with control plots (Fig. 1; 0 vs. A: $p = 1.000$ for ln(Aβ40/43), $p = 1.000$ for ln(Aβ38/42)). However, the γ-secretase activities differed between stage B specimens and 0/A specimens (0 vs. B: $p = 0.005$ for ln(Aβ40/43) and $p < 0.001$ for ln(Aβ38/42); A vs. B: $p = 0.002$ for ln(Aβ40/43) and $p = 0.001$ for ln(Aβ38/42); Fig. 1). AD (stage C) plots were shifted the most (0 vs. C: $p < 0.001$ for ln(Aβ40/43) and $p = 0.003$ for ln(Aβ38/42); A vs. C: $p < 0.001$ for ln(Aβ40/43) and $p = 0.007$ for ln(Aβ38/42)). Most interestingly, although AD plots were shifted to the same extent as stage B plots for Aβ38/42 (B vs. C: $p = 1.000$ for ln(Aβ38/42)), stage B and AD plots differ for Aβ40/43 (B vs. C: $p < 0.001$ for ln(Aβ40/43); Fig. 1).

Although these data were obtained from a cross-sectional study, one might assume that stage A develops through to stage B and eventually to stage C over decades (Duyckaerts and Hauw, 1997).

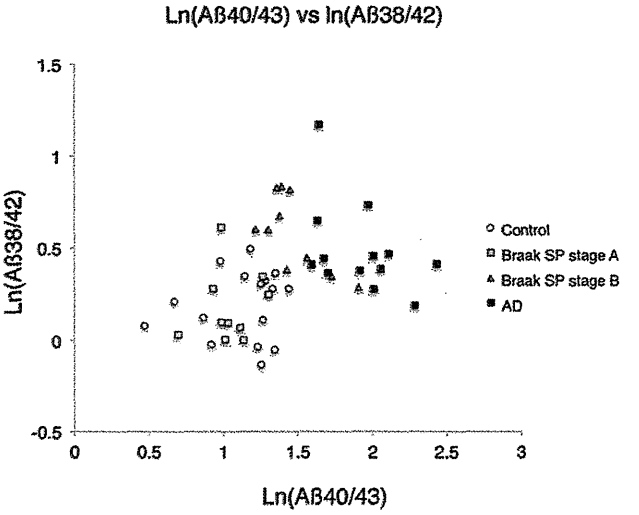

Fig. 1. Ln(amyloid-β protein [Aβ]40/43) versus ln(Aβ38/42) plot of raft-associated γ-secretase prepared from the brains in various (Braak) senile plaque (SP) stages. The raft-associated γ-secretase prepared from Braak SP stages 0, A, B, and C (AD) brain specimens were incubated with 200 nM of βCTF for 1 hour at 37 °C. After centrifugation of the reaction mixtures, the supernatants were saved for quantitative Western blot analysis of Aβs using specific antibodies.

Thus, the Aβ42 product line of γ-secretase appears to undergo changes early and the Aβ42-lowering activity remains constant through to development of AD. By contrast, the Aβ40 product line gradually changes with increasing Aβ40/43 ratio, as stage 0/A develops to stage B and finally to AD. Our previous observations showed that Aβ42 levels in CSF parallel the Aβ38/42 ratio, and Aβ43 levels parallel the Aβ40/43 ratio (Kakuda et al., 2012). These findings suggest that a decrease in the Aβ42 level would be the first alteration observable in CSF and that the level does not change throughout the disease course, whereas the Aβ43 level in CSF would decrease progressively up to AD.

We noted previously that the effects of Aβ42-lowering γ-modulators could be minimal in sporadic MCI/AD patients because modulation of γ-secretase has already begun in their brains. As mentioned above, the modulation of γ-secretase is evident in stage B. Accordingly, we investigated the response of γ-secretase to GSM-1, an Aβ42-lowering modulator, in control and AD brains. We reasoned that a strong response of the altered γ-secretase to GSM-1 would indicate that the drug might still be effective.

We quantified γ-secretase activities in the absence or presence of GSM-1 in control and AD specimens. This agent is known to aggressively modulate only conversion from Aβ42 to Aβ38, but not that from Aβ43 to Aβ40 (Crump et al., 2011; Ebke et al., 2011; Ohki et al., 2011). As expected, GSM-1 treatment significantly lowered Aβ42 and increased Aβ38 in control (see Supplementary Fig. 1). By contrast, in AD specimens, GSM-1 lowered Aβ42 and increased Aβ38 but to a lesser extent (Supplementary Fig. 1). The generation of Aβ40 and Aβ43, and the total production of Aβ were unchanged by the treatment of GSM-1 in all specimens (Supplementary Fig. 1).

In AD specimens, conversion of Aβ43 to Aβ40 seems to be altered compared with control (Kakuda et al., 2012), but this might be due to high concentrations of GSM-1 (>0.5 μM), which suppressed Aβ40 (and Aβ43) product line and total Aβ production in both control and AD specimens (data not shown). GSM-1 treatment significantly elevated the ratio of Aβ38/42 in control (Aβ38/42 with dimethyl sulfoxide vs. Aβ38/42 with GSM-1; $p < 0.000$, paired *t* test; Fig. 2A). By contrast, the same treatment of AD specimens

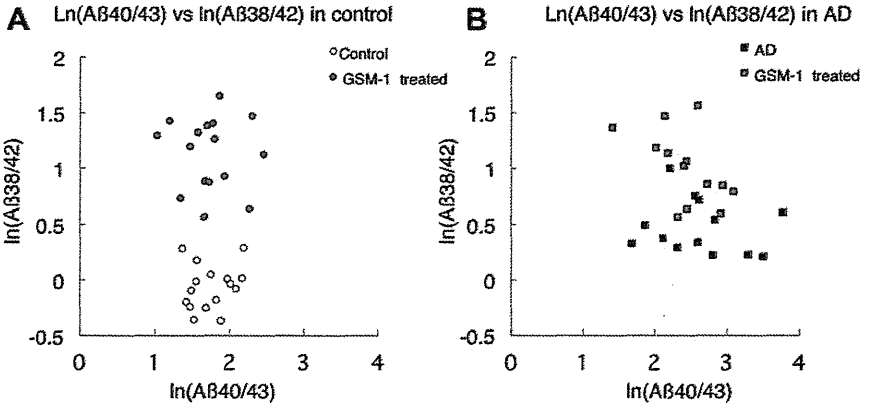

Fig. 2. Ln(amyloid-β protein [Aβ]40/43) versus ln(Aβ38/42) plot of γ-secretase modulator (GSM)-1-treated raft-associated γ-secretase activity. The raft-associated γ-secretases prepared from control (A) and AD (B) brains were incubated with 200 nM of βCTF for 1 hour at 37 °C in the presence of dimethyl sulfoxide or 0.3 μM GSM-1. Aβs produced were quantified by quantitative Western blot analysis using specific antibodies.

caused a much smaller increase in the Aβ38/42 ratio ($p < 0.001$ for AD paired t test; Fig. 2B). There was no significant difference in the Aβ40/43 ratio between control and AD specimens (Aβ40/43 with dimethyl sulfoxide vs. Aβ40/43 with GSM-1; $p = 0.814$ for control; $p = 0.223$ for AD, respectively; paired t test; Fig. 2A and B). The modulating effect on the Aβ38/42 ratio can be interpreted as indicating the extent of GSM-1-induced shift in the Aβ38/42 ratio (Supplementary Table 1). γ-Secretase was associated with significantly lower ratios in AD specimens than in control specimens (control vs. AD: $p < 0.001$), indicating a poor response to GSM-1 in AD specimens.

4. Discussion

Modulation of γ-secretase occurs in AD brains (Kakuda et al., 2012), and to a significant extent already at the stage of amyloid deposition, a decade or even decades before the onset of AD (Duyckaerts and Hauw, 1997). Although γ-secretase self-modulates and produces less Aβ42, it is likely that β-amyloid accumulation slowly progresses and ultimately extends throughout the brain, finally involving primary cortical centers (Duyckaerts and Hauw, 1997). A gradual decline in the rate of Aβ accumulation curve (Kawarabayashi et al., 2001) might be caused by self-modulation of γ-secretase. Currently, we do not know which comes first, Aβ deposition or γ-self-modulation. However, the efficacy of GSM-1 and γ-modulators in general would be limited when Aβ42 deposition and self-modulation of γ-secretase begins in the brain. To date, the efficacy of γ-modulators has been confirmed most often using younger Tg2576 mice, which do not yet accumulate Aβ (Borgegard et al., 2012; Kounnas et al., 2010). In Tg2576 mice, Aβ deposition starts at 9–12 months, and γ-secretase activity changes together with increasing Aβ deposition in the brain starting at 15–16 months of age (Kawarabayashi et al., 2001; data not shown). Thus, the true effectiveness of γ-modulators in Tg2576 mice should be assessed after 15–16 months of age. It is unclear whether γ-modulators are effective in such amyloid-bearing aged mice.

Disclosure statement

The authors have no conflict of interest.

Ethic permission was approved by Faculty of Life and Medical Sciences, Doshisha University, and we obtained written informed consent for their use for medical research from the patient or the patient's family.

Acknowledgements

The authors thank Dr Masayasu Okochi, Neuropsychiatry and Neurochemistry, Department of Integrated Medicine, Osaka University Graduate School of Medicine, for kindly providing GSM-1, and Dr Satoru Funamoto, Department of Neuropathology, Faculty of Life and Medical Sciences, Doshisha University, for providing βCTF. This project was supported in part by the New Energy and Industrial Technology Development Organization, Japan (J-ADNI) and by the MEXT-Supported Program for the Strategic Research Foundation at Private Universities, 2012–2017.

Appendix A. Supplementary data

Supplementary data associated with this article can be found, in the online version, at http://dx.doi.org/10.1016/j.neurobiolaging.2012.08.017.

References

Borgegard, T., Juréus, A., Olsson, F., Rosqvist, S., Sabirsh, A., Rotticci, D., Paulsen, K., Klintenberg, R., Yan, H., Waldman, M., Stromberg, K., Nord, J., Johansson, J., Regner, A., Parpal, S., Malinowsky, D., Radesater, A.C., Li, T., Singh, R., Eriksson, H., Lundkvist, J., 2012. First and second generation γ-secretase modulators (GSMs) modulate amyloid-β (Aβ) peptide production through different mechanisms. J. Biol. Chem. 287, 11810–11819.

Braak, H., Braak, E., 1991. Neuropathological stageing of Alzheimer-related changes. Acta Neuropathol. 82, 239–259.

Crump, C.J., Fish, B.A., Castro, S.V., Chau, D.M., Gertsik, N., Ahn, K., Stiff, C., Pozdnyakov, N., Bales, K.R., Johnson, D.S., Li, Y.M., 2011. Piperidine acetic acid based γ-secretase modulators directly bind to Presenilin-1. ACS Chem. Neurosci. 2, 705–710.

Duyckaerts, C., Hauw, J.J., 1997. Prevalence, incidence and duration of Braak's stages in the general population: can we know? Neurobiol. Aging 18, 362–369.

Ebke, A., Luebbers, T., Fukumori, A., Shirotani, K., Haass, C., Baumann, K., Steiner, H., 2011. Novel γ-secretase enzyme modulators directly target presenilin protein. J. Biol. Chem. 286, 37181–37186.

Fagan, A.M., Mintun, M.A., Mach, R.H., Lee, S.Y., Dence, C.S., Shah, A.R., LaRossa, G.N., Spinner, M.L., Klunk, W.E., Mathis, C.A., DeKosky, S.T., Morris, J.C., Holtzman, D.M., 2006. Inverse relation between in vivo amyloid imaging load and cerebrospinal fluid Abeta42 in humans. Ann. Neurol. 59, 512–519.

Iwatsubo, T., Odaka, A., Suzuki, N., Mizusawa, H., Nukina, N., Ihara, Y., 1994. Visualization of Aβ42(43) and Aβ40 in senile plaque with end-specific Aβ monoclonals: evidence that an initially deposited forms is Aβ42(43). Neuron 13, 45–53.

Kakuda, N., Shoji, M., Arai, H., Furukawa, K., Ikeuchi, T., Akazawa, K., Takami, M., Hatsuta, H., Murayama, S., Hashimoto, Y., Miyajima, M., Arai, H., Nagashima, Y., Yamaguchi, H., Kuwano, R., Nagaike, K., Ihara, Y., Japanese Alzheimer's Disease Neuroimaging Initiative, 2012. Altered γ-secretase activity in mild cognitive impairment and Alzheimer's disease. EMBO Mol. Med. 4, 344–352.

Kawarabayashi, T., Younkin, L.H., Saido, T.C., Shoji, M., Ashe, K.H., Younkin, S.G., 2001. Age-dependent changes in brain, CSF, and plasma amyloid (β) protein in the Tg2576 transgenic mouse model of Alzheimer's disease. J. Neurosci. 21, 372–381.

Kounnas, M.Z., Danks, A.M., Cheng, S., Tyree, C., Ackerman, E., Zhang, X., Ahn, K., Nguyen, P., Comer, D., Mao, L., Yu, C., Pleynet, D., Digregorio, P.J., Velicelebi, G., Stauderman, K.A., Comer, W.T., Mobley, W.C., Li, Y.M., Sisodia, S.S., Tanzi, R.E., Wagner, S.L., 2010. Modulation of gamma-secretase reduces beta-amyloid deposition in a transgenic mouse model of Alzheimer's disease. Neuron 67, 769–780.

Ohki, Y., Higo, T., Uemura, K., Shimada, N., Osawa, S., Berezovska, O., Yokoshima, S., Fukuyama, T., Tomita, T., Iwatsubo, T., 2011. Phenylpiperidine-type γ-secretase modulators target the transmembrane domain 1 of presenilin 1. EMBO J. 30, 4815–4824.

Selkoe, D.J., 2001. Alzheimer's disease: genes, proteins, and therapy. Physiol. Rev. 81, 741–766.

Serneels, L., Van Biervliet, J., Craessaerts, K., Dejaegere, T., Horré, K., Van Houtvin, T., Esselmann, H., Paul, S., Schäfer, M.K., Berezovska, O., Hyman, B.T., Sprangers, B., Sciot, R., Moons, L., Jucker, M., Yang, Z., May, P.C., Karran, E., Wiltfang, J., D'Hooge, R., De Strooper, B., 2009. γ-Secretase heterogeneity in the Aph1 subunit: relevance for Alzheimer's disease. Science 324, 639–642.

Sisodia, S.S., St George-Hyslop, P.H., 2002. gamma-Secretase, Notch, Abeta and Alzheimer's disease: where do the presenilins fit in? Nat. Rev. Neurosci. 3, 281–290.

Takami, M., Nagashima, Y., Sano, Y., Ishihara, S., Morishima-Kawashima, M., Funamoto, S., Ihara, Y., 2009. γ-Secretase: successive tripeptide and tetrapeptide release from the transmembrane domain of β-carboxyl terminal fragment. J. Neurosci. 29, 13042–13052.

Takasugi, N., Tomita, T., Hayashi, I., Tsuruoka, M., Niimura, M., Takahashi, Y., Thinakaran, G., Iwatsubo, T., 2003. The role of presenilin cofactors in the γ-secretase complex. Nature 422, 438–441.

Wakabayashi, T., De Strooper, B., 2008. Presenilins: members of the gamma-secretase quartets, but part-time soloists too. J. Physiol. 23, 194–204.

BMJ open accessible medical research

Multicentre multiobserver study of diffusion-weighted and fluid-attenuated inversion recovery MRI for the diagnosis of sporadic Creutzfeldt–Jakob disease: a reliability and agreement study

Koji Fujita,[1] Masafumi Harada,[2] Makoto Sasaki,[3] Tatsuhiko Yuasa,[4] Kenji Sakai,[5] Tsuyoshi Hamaguchi,[5] Nobuo Sanjo,[6] Yusei Shiga,[7] Katsuya Satoh,[8] Ryuichiro Atarashi,[8] Susumu Shirabe,[9] Ken Nagata,[10] Tetsuya Maeda,[10] Shigeo Murayama,[11] Yuishin Izumi,[1] Ryuji Kaji,[1] Masahito Yamada,[5] Hidehiro Mizusawa[6]

To cite: Fujita K, Harada M, Sasaki M, *et al*. Multicentre, multiobserver study of diffusion-weighted and fluid-attenuated inversion recovery MRI for the diagnosis of sporadic Creutzfeldt–Jakob disease: a reliability and agreement study. *BMJ Open* 2012;**2**: e000649. doi:10.1136/bmjopen-2011-000649

► Prepublication history for this paper is available online. To view this file please visit the journal online (http://bmjopen.bmj.com).

Received 21 November 2011
Accepted 20 December 2011

For numbered affiliations see end of article.

Correspondence to
Dr Masafumi Harada; masafumi@clin.med.tokushima-u.ac.jp

ABSTRACT

Objectives: To assess the utility of the display standardisation of diffusion-weighted MRI (DWI) and to compare the effectiveness of DWI and fluid-attenuated inversion recovery (FLAIR) MRI for the diagnosis of sporadic Creutzfeldt–Jakob disease (sCJD).

Design: A reliability and agreement study.

Setting: Thirteen MRI observers comprising eight neurologists and five radiologists at two universities in Japan.

Participants: Data of 1.5-Tesla DWI and FLAIR were obtained from 29 patients with sCJD and 13 controls.

Outcome measures: Standardisation of DWI display was performed utilising b0 imaging. The observers participated in standardised DWI, variable DWI (the display adjustment was observer dependent) and FLAIR sessions. The observers independently assessed each MRI for CJD-related lesions, that is, hyperintensity in the cerebral cortex or striatum, using a continuous rating scale. Performance was evaluated by the area under the receiver operating characteristics curve (AUC).

Results: The mean AUC values were 0.84 (95% CI 0.81 to 0.87) for standardised DWI, 0.85 (95% CI 0.82 to 0.88) for variable DWI and 0.68 (95% CI 0.63 to 0.72) for FLAIR, demonstrating the superiority of DWI ($p<0.05$). There was a trend for higher intraclass correlations of standardised DWI (0.74, 95% CI 0.66 to 0.83) and variable DWI (0.72, 95% CI 0.62 to 0.81) than that of FLAIR (0.63, 95% CI 0.53 to 0.74), although the differences were not statistically significant.

Conclusions: Standardised DWI is as reliable as variable DWI, and the two DWI displays are superior to FLAIR for the diagnosis of sCJD. The authors propose that hyperintensity in the cerebral cortex or striatum on 1.5-Tesla DWI but not FLAIR can be a reliable diagnostic marker for sCJD.

ARTICLE SUMMARY

Article focus

- Evaluation of the reliability of diffusion-weighted imaging (DWI) display standardisation for the diagnosis of sporadic Creutzfeldt–Jakob disease (sCJD).
- Comparison between DWI and fluid-attenuated inversion recovery (FLAIR) for the diagnosis of sCJD.

Key messages

- Standardised DWI display is as reliable as observer-dependent DWI display.
- DWI is superior to FLAIR for the diagnosis of sCJD.
- Hyperintensity in the cerebral cortex or striatum on 1.5-Tesla DWI but not FLAIR can be a reliable diagnostic marker for sCJD.

Strengths and limitations of this study

- Strength of this study is the large number of physicians who participated in the observer performance study.
- This study was limited by the retrospective nature that may lead to a selection bias.

INTRODUCTION

Reliable detection of Creutzfeldt–Jakob disease (CJD) is imperative for infection control and treatment. MRI is useful for the early diagnosis of CJD,[1 2] whereas the utility of EEG and conventional cerebrospinal fluid (CSF) tests have been limited.[3] Diffusion-weighted imaging (DWI) and fluid-attenuated inversion recovery (FLAIR) are key techniques for the diagnosis of sporadic CJD (sCJD) with high sensitivity and specificity when assessed by expert neurologists or

neuroradiologists.[1 4 5] However, the utility of MRI for general neurologists or radiologists who are not familiar with diagnosing CJD remains elusive. Moreover, standardisation of MRI methodologies, which would be essential for the reproducible assessment of MRI findings of CJD cases, has not been achieved in previous studies.[1 4 5] DWI display conditions may particularly vary among institutions or operators,[6] which can give rise to inaccurate assessment of CJD-related lesions, specifically subtle abnormalities in the cerebral cortex. Meanwhile, although DWI seems superior to FLAIR for the detection of CJD lesions,[5] direct comparison of the two sequences is yet to be performed.

To address these issues, we investigated the utility of a newly proposed standardisation method of DWI display[6 7] and compared the effectiveness of DWI and FLAIR for the diagnosis of sCJD, particularly for differentiating between abnormal and normal signals by neurologists and radiologists who are not necessarily CJD experts. We conducted a multicentre, multiobserver case–control study and evaluated observer performance with receiver operating characteristics (ROC) analysis.

METHODS

Subjects

Patients diagnosed as having sCJD by the CJD Surveillance Committee of Japan[8] from October 2005 to September 2010 were eligible to participate in this study. The accuracy of the diagnosis was defined as follows: definite, that is, pathologically verified cases; probable, that is, cases with neuropsychiatric manifestations compatible with sCJD and periodic sharp wave complexes on EEG without pathological examinations and possible, that is, cases with the same findings as probable sCJD but no periodic sharp wave complexes on EEG.[8 9] WHO criteria[10] were not applied because the assay of CSF 14-3-3 protein, which is required by WHO criteria, was standardised only since April 2009 in Japan.[11] The prion protein gene (*PRNP*) was analysed in the open reading frame after extracting DNA from patients' blood.[12 13] For neuropathological examinations, brain sections were stained with routine techniques, and immunohistochemistry was performed using the mouse monoclonal antibody 3F4 (Senetek, MD Heights, Missouri, USA).[12] For PrP^{Sc} typing, frozen brain tissues were homogenised and analysed by western blot for proteinase K-resistant PrP using the 3F4 antibody.[14] Assays for CSF γ-isoform of 14-3-3 protein,[11] total τ protein (cut-off value, 1300 pg/ml)[15] and real-time quaking-induced conversion (RT-QUIC)[16] were performed in patients whose CSF samples were available. The following patients were eligible as disease controls: patients who were suspected to have prion disease by primary physicians but were denied to have prion disease by the Committee or those who were diagnosed as having other neurological disorders at Tokushima University Hospital and whose brain MRI showed no abnormal intensity in the cerebral cortex or striatum. We requested physicians who had referred patients to the Committee to provide initial MRI data of eligible patients.

This study was approved by the Medical Ethics Committee of Kanazawa University and the Ethics Committees of the Tokushima University Hospital and Tokyo Medical and Dental University. Written informed consent was obtained from all patients or their families.

Magnetic resonance imaging

DWI, b0 and FLAIR images were converted to the Digital Imaging and Communication in Medicine format. When the Digital Imaging and Communication in Medicine data contained patient information, it was excluded by one of the investigators (MH) before the observer performance study. All MRI studies were performed on 1.5-Tesla scanners at each hospital. Quadrature detection head coils or multichannel head coils were used. DWI was performed using the single-shot spin-echo echo planar imaging technique with the following parameters: repetition time, 4000–8000 ms; echo time, 70–100 ms; b value, 1000 s/mm^2; slice thickness, 5 mm; matrix size, 128×80 to 128×128; field of view, 220–230 mm and 16–20 contiguous axial sections parallel to a line through the anterior and posterior commissures were obtained from each patient. The scanning parameters of FLAIR were as follows: repetition time, 8000–10 000 ms; inversion time, 2000–2500 ms; effective echo time, 105–120 ms; matrix size, 256×192 to 320×224; field of view, 210–220 mm; slice thickness, 5–6 mm with 1–1.5 mm interslice gaps and 19–20 slices per patient.

Display methods

Two display methods were used for DWI: standardised and variable. In the standardised display, the window width and level settings were constant for all evaluations and could not be changed. Details of the standardised display have been reported elsewhere.[6] In brief, the window width and level were as follows: window width = SI_{b0} and window level = $SI_{b0}/2$, where SI_{b0} represents the signal intensity in the normal-appearing subcortical region on b0 imaging.[6] One radiologist (MH) manually measured SI_{b0} within a circular region of interest. The calculated window width and level were applied to all images. In the variable display mode, regarded as the most reliable for assessment of DWI, each observer was able to change the window width and level settings on the monitor according to preference. FLAIR was assessed with the variable display method because no standardised methods are currently available for FLAIR display.

Observer performance study

Eight neurologists (6–27 years of experience; mean, 12 years; board certified, six) and five radiologists (5–25 years of experience; mean, 12.8 years; board certified, four; neuroradiologist, one) participated in the observer performance study at The University of Tokushima Graduate School (persons, six; neurologists, three) and Tokyo Medical and Dental University

(persons, seven; neurologists, five including NS and YS). Before the test, the observers were informed that the purpose of the study was to evaluate their performance in detecting MRI lesions compatible with CJD, that is, hyperintensity in the cerebral cortex or striatum, regardless of signal changes in other regions including the thalamus. Three sessions were conducted: standardised DWI, variable DWI and FLAIR. To reduce the effect of learning, the interval between reading sessions was 1 week or longer. The order of the three sessions was randomised among the observers. Using computer randomisation, images of patients with and without sCJD were intermixed. All cases were presented in the same randomised order to the observers in each session. Each observer independently viewed all slices of each MRI study on the same type of monitors (Let'snote, Panasonic, Osaka, Japan) using INTAGE Realia Professional (Cubernet, Tokyo, Japan) run on Windows XP (Microsoft). The observers were allowed to adjust the window width and level only in variable DWI and FLAIR sessions but not in the standardised DWI session. Observers were blinded to any clinical information including age, sex and diagnosis.

Each observer used a continuous rating scale of a line-marking method to rate his or her confidence level on the paper format independently. At the left end of the line, a confidence level that lesions compatible with CJD were definitely absent was indicated, whereas at the right end, a confidence level that lesions were definitely present was indicated. Intermediate levels of confidence were indicated by the different positions on the line between the two ends. The distance between the left end and the marked point was converted to a confidence level that could range from 0 to 100, as described elsewhere.[17]

Statistical analyses

Observer performance was evaluated using ROC analysis with SPSS V.19 (IBM). The ROC curves for each observer indicated the ratio of the true-positive fraction to the false-positive fraction at each confidence level. The area under the ROC curve (AUC) was used to compare observer performance for accurately detecting CJD lesions. Intraclass correlations were calculated in the neurologist group, the radiologist group and for all observers by two-way random consistency measures using the SPSS software. In all the analyses, p values of <0.05 were considered statistically significant.

RESULTS

Patients and controls

MRI data from 85 patients were provided. Of these, 42 subjects from 15 hospitals (including authors' institutions) were eligible for this study after excluding cases that were diagnosed as having non-sporadic CJD or lacked the required MRI sequences. This study cohort included 29 patients with sCJD (men, 11; mean age, 71 years; duration before MRI, 4.4±6.1 months), three patients who were suspected of CJD but eventually diagnosed as negative by the Committee and 10 patients diagnosed as having other neurological disorders. Of the 29 sCJD patients, four had definite, 24 had probable and one had possible CJD. Twenty-six cases underwent *PRNP* analysis, 24 were homozygous for methionine at codon 129 and two were heterozygous with methionine and valine at codon 129. Of the four definite cases, PrP^{Sc} was type 1 in two cases, type 1+2 in one case and type 2 in one case. Eleven of 15 CSF samples from probable sCJD cases were positive for PrP^{Sc} by RT-QUIC (table 1).

Diagnoses for three prion-denied patients were immune-mediated encephalopathy, juvenile Alzheimer's disease and frontotemporal dementia. Other neurological controls were diagnosed with Alzheimer's disease, Parkinson's disease, spinocerebellar degeneration, vascular dementia, old cerebral infarction, benign paroxysmal positional vertigo, dizziness, temporal arteritis, cervical spondylosis and diabetic neuropathy.

Diagnostic performance

We investigated the diagnostic performance of standardised DWI, variable DWI and FLAIR images assessed by eight neurologists and five radiologists using ROC analysis. Mean AUC values obtained from the three sessions were compared within the neurologist group, the radiologist group and all observers (figure 1, table 2). The AUC values for standardised and variable DWI were not different within each professional group or for the total observer group. On the other hand, AUC values for FLAIR were significantly lower than DWI displayed by either method ($p<0.05$). Representative MRI scans are shown in figure 2.

Rating agreement

To measure the extent to which the observers agreed when rating the MRI findings, intraclass correlations were calculated. The intraclass correlations of the standardised DWI (0.74, 95% CI 0.66 to 0.83) and variable DWI (0.72. 95% CI 0.62 to 0.81) tend to be higher than that of FLAIR (0.63, 95% CI 0.53 to 0.74), specifically in the neurologist group, although the differences were not significant (figure 3).

DISCUSSION

We demonstrated that standardised DWI was as useful as variable DWI and that both DWI displays are superior to FLAIR for the diagnosis of sCJD when assessed by multiobservers with various specialty backgrounds.

Our standardisation method of DWI display was originally proposed as an easy-to-use way to decide the window width and level for DWI even in emergency settings.[6] Indeed, this method was demonstrated as useful for detecting acute ischaemic lesions on DWI.[7] Results of the present study show that the standardisation method is also reliable for diagnosis of sCJD, in which DWI is one of the key sequences. We suggest some advantages of standardised DWI over variable DWI, although there was no statistical difference between the two methods. First, standardised DWI can be helpful for

Table 1 Clinical profiles of patients with sporadic Creutzfeldt–Jakob disease

No	Age/sex	Diagnosis	Codon129/PrP^{Sc}	14-3-3/total τ	RT-QUIC	Pre-MRI duration (months)
1	69/M	Definite	MM/1	+/+	+	–2*
2	77/F	Definite	MM/1	+/+	+	19
3	75/F	Definite	ND/1+2	+/+	+	3
4	65/M	Definite	MM/2	–/–	–	12
5	69/M	Probable	MM	ND	–	0.5
6	72/F	Probable	MM	ND	ND	0.5
7	77/F	Probable	MM	–/–	+	0.5
8	72/M	Probable	MM	ND	ND	1
9	63/M	Probable	MM	+/+	+	1.5
10	88/F	Probable	MM	ND	ND	1.5
11	75/M	Probable	MV	ND	ND	1.5
12	56/M	Probable	MM	+/+	+	2
13	67/M	Probable	MM	+/+	–	2
14	70/M	Probable	MM	+/+	+	2
15	70/F	Probable	MM	+/+	+	2
16	74/F	Probable	MM	+/+	–	2
17	84/F	Probable	MM	+/–	+	2
18	85/F	Probable	MM	–/+	+	2
19	49/F	Probable	ND	+/+	+	2
20	74/F	Probable	MV	+/+	+	2.5
21	54/F	Probable	ND	ND	ND	2.5
22	61/M	Probable	MM	ND	ND	3
23	72/F	Probable	MM	+/–	–	3
24	81/F	Probable	MM	–/–	+	3
25	70/M	Probable	MM	+/+	+	6
26	83/F	Probable	MM	+/+	ND	9
27	67/F	Probable	MM	+/+	–	15
28	84/F	Probable	MM	+/+	–	26
29	57/F	Possible	MM	ND	ND	4

*MRI was obtained 2 months before the symptom onset.[2]
MM, homozygous for methionine; MV, heterozygous with methionine and valine; ND, not done; RT-QUIC, real-time quaking-induced conversion.

physicians who can refer only to hardcopies but not softcopies. Second, even for doctors who can readily refer to softcopies and thus variable DWI, the standardisation method can simplify assessment procedure without any disadvantages. Third, the standardisation can facilitate direct comparison of DWI findings from different CJD patients.

DWI and FLAIR have been reported as useful markers for the diagnosis of CJD. Of these, DWI has been assumed to be the most sensitive, although without direct evidence.[1 5 18] Hyperintensity in the cerebral cortices, the striatum or both indicates the diagnosis of CJD. The striatum hyperintensity is anterior dominant at early stages of the disease.[19] MRI lesion profiles reportedly differ among molecular subtypes of sCJD,[20 21] which was not reproduced in a recent study.[5] Zerr *et al*[4] proposed that high-signal abnormalities in caudate nucleus and putamen or at least two cortical regions (temporal, parietal or occipital lobes) either in DWI or FLAIR together with typical clinical signs can be diagnostic for probable sCJD. Based partly upon their report, 'high signal in caudate/putamen on MRI brain scan' has

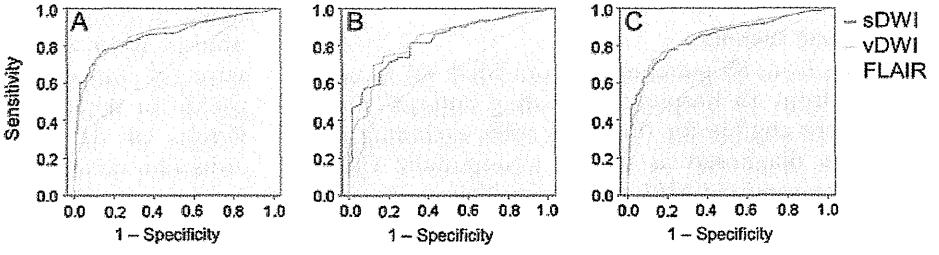

Figure 1 Receiver operating characteristic curves for each display in diagnosis of sporadic Creutzfeldt–Jakob disease. (A) Neurologists, (B) radiologists and (C) all observers. The true rate (sensitivity) is plotted as a function of the false-positive rate (1 – specificity). DWI, diffusion-weighted imaging; FLAIR, fluid-attenuated inversion recovery; sDWI, standardised DWI; vDWI, variable DWI.

Table 2 Areas under the receiver operating characteristic curves

	Neurologists	Radiologists	All observers
sDWI	0.86 (0.82 to 0.90)	0.82 (0.77 to 0.88)	0.84 (0.81 to 0.87)
vDWI	0.86 (0.82 to 0.90)	0.83 (0.77 to 0.89)	0.85 (0.82 to 0.88)
FLAIR	0.69 (0.63 to 0.75)	0.66 (0.58 to 0.73)	0.68 (0.63 to 0.72)

Means (95% CIs) are indicated.
DWI, diffusion-weighted imaging; FLAIR, fluid-attenuated inversion recovery; sDWI, standardised DWI; vDWI, variable DWI.

been used as one of the laboratory findings in the diagnostic criteria for probable sCJD in the European CJD Surveillance System (EUROCJD) since January 2010.[22] However, their criteria did not distinguish DWI and FLAIR, thereby maintaining ambiguity about the diagnostic values of MRI in situations where DWI is not available. Our data indicate that FLAIR without DWI is unreliable for the diagnosis of sCJD. On the other hand, high signals in the cerebral cortex have not been regarded as diagnostic in the EUROCJD criteria, probably because cortical abnormalities are less reliable on conventional MRI. Our results suggest that, using standardised or variable DWI but not FLAIR, cortical signals can also be used as a diagnostic marker.

Meanwhile, Young *et al*[23] reported that the sensitivity and the specificity of DWI and FLAIR for the diagnosis of CJD are 91% and 95%, respectively. More recently, Vitali *et al*[5] reported that hyperintensity greater on DWI than FLAIR is diagnostic for sCJD, whereas hyperintensity greater on FLAIR than DWI is characteristic for non-prion rapidly progressive dementia. Furthermore, reduction of apparent diffusion coefficient in subcortical (striatum) hyperintensity regions on DWI is supportive for sCJD.[5 24 25] These findings can be greatly helpful for differentiating sCJD from other rapidly progressive dementia. However, assessment of FLAIR lesions tends to vary among physicians, particularly among neurologists, as shown by the present study, and standardised methods for FLAIR or apparent diffusion coefficient map have not been established until date. Therefore, clinical criteria which require DWI but not necessarily FLAIR or apparent diffusion coefficient will be more readily applicable.

As many as 13 neurologists and radiologists from different institutions participated in the observer performance study, although the sample size of patients was relatively small. Notably, the observers had various specialty backgrounds such as stroke neurologists, neurophysiologists, experts in dementia or prion disease and general and neuroradiologists. This variety simulates practical situations in which the diagnosis of suspected CJD cases may be made by physicians who do not necessarily specialise in prion disease.

This study has some limitations. First, we did not evaluate patterns of cortical involvement suggestive of sCJD[4 5] because we had to address whether DWI or FLAIR is suitable for detecting cortical lesions in the first place. Second, we did not assess the difference among sCJD subtypes[21] because majority of our cases had a typical phenotype and were homozygous for methionine; thus, they were compatible with MM1 sCJD. Until date, MM2 thalamic-type sCJD remains a diagnostic challenge in MRI-based assessment; thalamic hypoperfusion or hypometabolism on SPECT or PET can be useful.[26] Third, majority of the control patients were not those who were suspected to have CJD. However, the

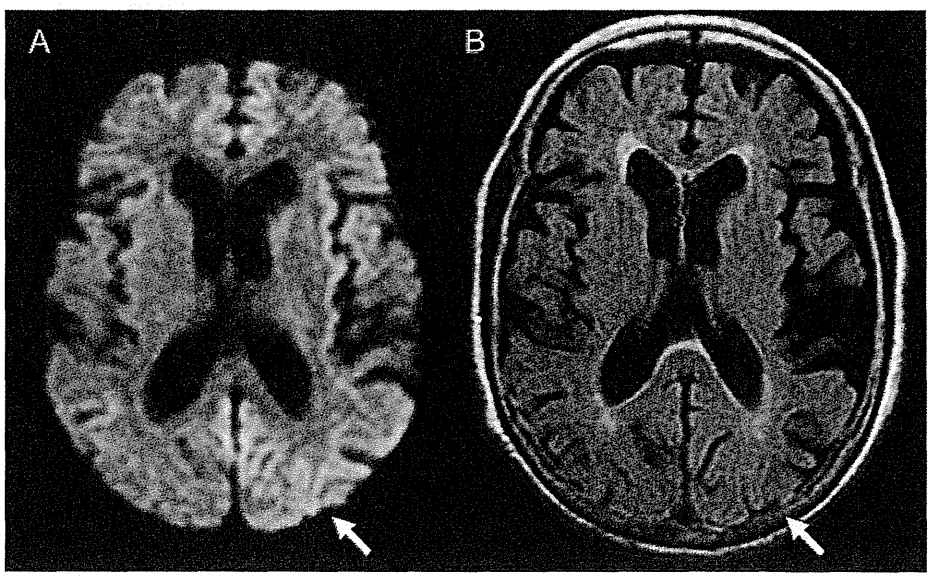

Figure 2 Representative MRI of a sporadic Creutzfeldt–Jakob disease patient (case 17). Abnormal hyperintensity in the cerebral cortex is evident on standardised diffusion-weighted imaging (A, arrow) but obscure on fluid-attenuated inversion recovery (B, arrow).

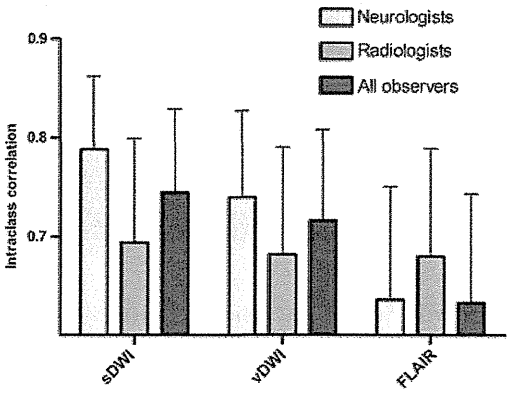

Figure 3 Intraclass correlations for each display. Error bars represent upper limits of 95% CIs. DWI, diffusion-weighted imaging; FLAIR, fluid-attenuated inversion recovery; sDWI, standardised DWI; vDWI, variable DWI.

principle aim of the present study was to establish a display method, which reliably distinguishes potentially CJD-associated signals from normal signals. Thus, our results provide a practical foundation for utilising DWI as a general diagnostic marker of sCJD when combined with previous findings.[1 4 5]

Although neuropathological confirmation of the diagnosis of sCJD was obtained in few cases, we performed RT-QUIC, a newly established CSF PrP^{Sc} amplification assay which achieved >80% sensitivity and 100% specificity for CJD.[16] Overall, 15 of 29 cases (51.7%) were pathologically proven or confirmed by RT-QUIC to have CJD. There were no significant differences in MRI findings between sCJD patients with and without positive results of CSF 14-3-3 protein, total τ protein or RT-QUIC. It will be important to further evaluate accurate diagnostic ability (sensitivity and specificity) of DWI in a prospective cohort of suspected CJD patients, that is, consecutive patients registered to the CJD surveillance who will also undergo CSF confirmation tests or neuropathological analyses.

In conclusion, we suggest that hyperintensity in the cerebral cortex or striatum assessed on the standardised or variable DWI scanned with 1.5-Tesla machines can be a reliable first-line on-site diagnostic marker for sCJD.

Author affiliations
[1]Department of Clinical Neuroscience, Institute of Health Biosciences, The University of Tokushima Graduate School, Tokushima, Japan
[2]Department of Radiology, Institute of Health Biosciences, The University of Tokushima Graduate School, Tokushima, Japan
[3]Advanced Medical Science Center, Iwate Medical University, Morioka, Japan
[4]Department of Neurology, Kamagaya-Chiba Medical Center for Intractable Neurological Disease, Kamagaya General Hospital, Kamagaya, Japan
[5]Department of Neurology and Neurobiology of Aging, Kanazawa University Graduate School of Medical Science, Kanazawa, Japan
[6]Department of Neurology and Neurological Science, Graduate School, Tokyo Medical and Dental University, Tokyo, Japan
[7]Department of Neurology, Aoba Neurosurgical Clinic, Sendai, Japan
[8]Department of Molecular Microbiology and Immunology, Nagasaki University Graduate School of Biomedical Sciences, Nagasaki, Japan
[9]Center for Health and Community Medicine, Nagasaki University, Nagasaki, Japan
[10]Department of Neurology, Research Institute for Brain and Blood Vessels, Akita, Japan
[11]Department of Neuropathology (Brain Bank for Aging Research), Tokyo Metropolitan Institute of Gerontology, Tokyo, Japan

Acknowledgements We thank Tetsuyuki Kitamoto (Tohoku University Graduate School of Medicine) for *PRNP* analysis, western blotting of PrP and neuropathological investigations; Yuka Terasawa, Yoshimitsu Shimatani, Ai Miyashiro (Department of Clinical Neuroscience, The University of Tokushima Graduate School), Hideki Otsuka, Naomi Morita, Yoichi Otomi (Department of Radiology, The University of Tokushima Graduate School), Satoru Ishibashi, Takumi Hori, Akira Machida (Department of Neurology and Neurological Science, Tokyo Medical and Dental University), Isamu Ohashi and Takashi Katayama (Department of Radiology, Tokyo Medical and Dental University) for participation in the observer performance study. We also thank Joe Senda (Nagoya University), Yuko Nemoto (Chiba Medical Center), Akio Kawakami (Kaetsu Hospital), Isao Sasaki (Mizunomiyako Memorial Hospital), Shigeyuki Kojima (Matsudo Municipal Hospital), Motohiro Yukitake (Saga University), Hiroyuki Murai (Iizuka Hospital), Hideki Mizuno (Kohnan Hospital), Akira Arai (Aomori Prefectural Central Hospital), Masamitsu Yaguchi (Shinoda General Hospital), Takanori Oikawa (South Miyagi Medical Center) and all other collaborative physicians for providing MRI data of the patients. We thank the members of the CJD Surveillance Committee of Japan for their support of this work.

Funding This study was supported by Grants-in-Aid from the Research Committee of Surveillance and Infection Control of Prion Disease and from the Research Committee of Prion Disease and Slow Virus Infection, the Ministry of Health, Labour and Welfare of Japan.

Competing interests None.

Patient consent Obtained.

Ethics approval This study was approved by the Medical Ethics Committee of Kanazawa University and the Ethics Committees of the Tokushima University Hospital and Tokyo Medical and Dental University.

Contributors KF, MH, MS, TY, KSak, TH, NS, YS, KSat, SS, MY and HM: design/conceptualisation of the study. MH, KSak, TH, NS, YS, KSat, RA, KN, TM, SM and YI: acquisition of data. KF, MH, MS, RA, RK, MY and HM: analysis/interpretation of the data. MH: statistical analyses. KF, MH, MS, TY, KSak, TH, NS, YS, KSat, RA, SS, KN, TM, SM, YI, RK, MY and HM: drafting/revising the manuscript. All authors contributed to final approval of the version to be published.

Provenance and peer review Not commissioned; externally peer reviewed.

Data sharing statement There are no additional data available.

REFERENCES

1. Shiga Y, Miyazawa K, Sato S, *et al.* Diffusion-weighted MRI abnormalities as an early diagnostic marker for Creutzfeldt–Jakob disease. *Neurology* 2004;63:443–9.
2. Satoh K, Nakaoke R, Nishiura Y, *et al.* Early detection of sporadic CJD by diffusion-weighted MRI before the onset of symptoms. *J Neurol Neurosurg Psychiatry* 2011;82:942–3.
3. Chitravas N, Jung RS, Kofskey DM, *et al.* Treatable neurological disorders misdiagnosed as Creutzfeldt–Jakob disease. *Ann Neurol* 2011;70:437–44.
4. Zerr I, Kallenberg K, Summers DM, *et al.* Updated clinical diagnostic criteria for sporadic Creutzfeldt–Jakob disease. *Brain* 2009;132:2659–68.
5. Vitali P, Maccagnano E, Caverzasi E, *et al.* Diffusion-weighted MRI hyperintensity patterns differentiate CJD from other rapid dementias. *Neurology* 2011;76:1711–19.
6. Sasaki M, Ida M, Yamada K, *et al.* Standardizing display conditions of diffusion-weighted images by using concurrent b0 images: a multivendor multi-institutional study. *Magn Reson Med Sci* 2007;6:133–7.
7. Hirai T, Sasaki M, Meada M, *et al*; Acute Stroke Imaging Standardization Group-Japan (ASIST-Japan). Diffusion-weighted imaging in ischemic stroke: effect of display method on observers' diagnostic performance. *Acad Radiol* 2009;16:305–12.
8. Nozaki I, Hamaguchi T, Sanjo N, *et al.* Prospective 10-year surveillance of human prion diseases in Japan. *Brain* 2010;133:3043–57.
9. Masters CL, Harris JO, Gajdusek DC, *et al.* Creutzfeldt–Jakob disease: patterns of worldwide occurrence and the significance of familial and sporadic clustering. *Ann Neurol* 1979;5:177–88.

10. WHO. Global surveillance, diagnosis and therapy of human transmissible spongiform encephalopathies: report of a WHO consultation. *World Health Organization: Emerging and Other Communicable Diseases, Surveillance and Control.* Geneva: WHO, 1998.
11. Satoh K, Tobiume M, Matsui Y, *et al.* Establishment of a standard 14-3-3 protein assay of cerebrospinal fluid as a diagnostic tool for Creutzfeldt–Jakob disease. *Lab Invest* 2010;90:1637–44.
12. Kitamoto T, Shin RW, Doh-ura K, *et al.* Abnormal isoform of prion proteins accumulates in the synaptic structures of the central nervous system in patients with Creutzfeldt–Jakob disease. *Am J Pathol* 1992;140:1285–94.
13. Kitamoto T, Ohata M, Doh-ura K, *et al.* Novel missense variants of prion protein in Creutzfeldt–Jakob disease or Gerstmann-Sträussler syndrome. *Biochem Biophys Res Commun* 1993;191:709–14.
14. Shimizu S, Hoshi K, Muramoto T, *et al.* Creutzfeldt–Jakob disease with florid-type plaques after cadaveric dura mater grafting. *Arch Neurol* 1999;56:357–62.
15. Satoh K, Shirabe S, Eguchi H, *et al.* 14-3-3 protein, total tau and phosphorylated tau in cerebrospinal fluid of patients with Creutzfeldt–Jakob disease and neurodegenerative disease in Japan. *Cell Mol Neurobiol* 2006;26:45–52.
16. Atarashi R, Satoh K, Sano K, *et al.* Ultrasensitive human prion detection in cerebrospinal fluid by real-time quaking-induced conversion. *Nat Med* 2011;17:175–8.
17. Hirai T, Korogi Y, Arimura H, *et al.* Intracranial aneurysms at MR angiography: effect of computer-aided diagnosis on radiologists' detection performance. *Radiology* 2005;237:605–10.
18. Kallenberg K, Schulz-Schaeffer WJ, Jastrow U, *et al.* Creutzfeldt–Jakob disease: comparative analysis of MR imaging sequences. *AJNR Am J Neuroradiol* 2006;27:1459–62.
19. Murata T, Shiga Y, Higano S, *et al.* Conspicuity and evolution of lesions in Creutzfeldt–Jakob disease at diffusion-weighted imaging. *AJNR Am J Neuroradiol* 2002;23:1164–72.
20. Parchi P, Giese A, Capellari S, *et al.* Classification of sporadic Creutzfeldt–Jakob disease based on molecular and phenotypic analysis of 300 subjects. *Ann Neurol* 1999;46:224–33.
21. Meissner B, Kallenberg K, Sanchez-Juan P, *et al.* MRI lesion profiles in sporadic Creutzfeldt–Jakob disease. *Neurology* 2009;72:1994–2001.
22. Diagnostic criteria for sporadic CJD from 1 January 2010. *National Creutzfeldt–Jakob Disease Surveillance Diagnostic Criteria [online].* http://www.cjd.ed.ac.uk/criteria.htm (accessed 3 Oct 2011).
23. Young GS, Geschwind MD, Fischbein NJ, *et al.* Diffusion-weighted and fluid-attenuated inversion recovery imaging in Creutzfeldt–Jakob disease: high sensitivity and specificity for diagnosis. *AJNR Am J Neuroradiol* 2005;26:1551–62.
24. Lin YR, Young GS, Chen NK, *et al.* Creutzfeldt–Jakob disease involvement of rolandic cortex: a quantitative apparent diffusion coefficient evaluation. *AJNR Am J Neuroradiol* 2006;27:1755–9.
25. Fujita K, Nakane S, Harada M, *et al.* Diffusion tensor imaging in patients with Creutzfeldt–Jakob disease. *J Neurol Neurosurg Psychiatry* 2008;79:1304–6.
26. Hamaguchi T, Kitamoto T, Sato T, *et al.* Clinical diagnosis of MM2-type sporadic Creutzfeldt–Jakob disease. *Neurology* 2005;64:643–8.

J Neuropathol Exp Neurol

Vol. 71, No. 8
August 2012
pp. 750–759

ORIGINAL ARTICLE

Characteristics of Aquaporin Expression Surrounding Senile Plaques and Cerebral Amyloid Angiopathy in Alzheimer Disease

Akihiko Hoshi, MD, PhD, Teiji Yamamoto, MD, PhD, Keiko Shimizu, MT, Yoshikazu Ugawa, MD, PhD, Masatoyo Nishizawa, MD, PhD, Hitoshi Takahashi, MD, PhD, and Akiyoshi Kakita, MD, PhD

Abstract

Senile plaques (SPs) containing amyloid β peptide (Aβ) 1–42 are the major species present in Alzheimer disease (AD), whereas Aβ1–40 is the major constituent of arteriolar walls affected by cerebral amyloid angiopathy. The water channel proteins astrocytic aquaporin 1 (AQP1) and aquaporin 4 (AQP4) are known to be abnormally expressed in AD brains, but the expression of AQPs surrounding SPs and cerebral amyloid angiopathy has not been described in detail. Here, we investigated whether AQP expression is associated with each species of Aβ deposited in human brains affected by either sporadic or familial AD. Immunohistochemical analysis demonstrated more numerous AQP1-positive reactive astrocytes in the AD cerebral cortex than in controls, located close to Aβ42- or Aβ40-positive SPs. In AD cases, however, AQP1-positive astrocytes were not often observed in Aβ-rich areas, and there was a significant negative correlation between the levels of AQP1 and Aβ42 assessed semiquantitatively. We also found that Aβ plaque-like AQP4 was distributed in association with Aβ42- or Aβ40-positive SPs and that the degree of AQP4 expression around Aβ40-positive vessels was variable. These findings suggest that a defined population of AQP1-positive reactive astrocytes may modify Aβ deposition in the AD brain, whereas the Aβ deposition process might alter astrocytic expression of AQP4.

Key Words: Amyloid-β peptides 42 and 40, Aquaporin 1, Aquaporin 4, Alzheimer disease, Cerebral amyloid angiopathy, Senile plaques.

INTRODUCTION

Alzheimer disease (AD) is characterized pathologically by abnormal accumulation of extracellular aggregates of amyloid-β peptide (Aβ) in the form of senile plaques (SPs) (1). A major component of these SPs is Aβ 1–42 (Aβ42), and the presence of Aβ 1–40 (Aβ40)–positive amyloid seems to be related to the development of SPs (2). Although they differ in only 2 amino acid residues at the C-terminal end, Aβ42 shows a stronger tendency to aggregate and is more toxic to neurons than Aβ40 (3). On the other hand, the major vascular pathology in AD is cerebral amyloid angiopathy (CAA), which results from Aβ40 deposition in arteriolar media (1, 4). Proportions of vessels containing Aβ40 deposits varied considerably among AD cases, and the severity of AD is not correlated with the extent of parenchymal Aβ deposition (1, 5). Despite extensive studies, how SPs and CAA are formed or degraded and how they relate to AD pathogenesis are still unclear.

The role of astroglia in Aβ processing and metabolism also remains unclear, but reactive astrocytosis in AD suggests their participation in the clearance and degradation of Aβ (6–9). Indeed, reactive astrocytes often surround SPs or CAA in AD brains; thus, they seem to regulate Aβ deposition (10, 11). Several recent studies have demonstrated that some of the water channel proteins, astrocytic aquaporin 1 (AQP1) and/or aquaporin 4 (AQP4), are abnormally expressed in AD brains (12–15). AQP1 is normally expressed in the apical membrane of the choroid plexus and participates in the formation of cerebrospinal fluid (16–19). AQP4 shows polarized localization in astrocyte foot processes where it is involved in brain edema formation in cases of stroke, brain tumor, acute bacterial meningitis, and brain abscess (18–23).

Differences between astrocytic AQP1 and AQP4 expression around SPs and CAA have not been investigated in detail. Thus, the precise roles of AQP expression in AD remain unknown. Because these channels are often localized near sites of Aβ deposition, we hypothesized that they might play a pivotal role in the degenerative processes of AD by modifying Aβ pathology. Therefore, we investigated whether AQP1 or AQP4 expression was associated with deposition of each Aβ species in human brains with advanced AD.

MATERIALS AND METHODS

Neuropathologic Assessment

Informed consent for research on all brain tissue was obtained from the Brain Research Institute, University of Niigata. The study was approved by the Ethics Committee of Fukushima Medical University. Autopsied brains of 8 patients with AD (5 with sporadic AD [sAD] and 3 with familial AD [fAD]) were examined and compared with the brains of 5 age-matched controls experiencing nonneurologic conditions. Each diagnosis was based on both clinical history and postmortem neuropathologic verification (24). Clinical data for the 13 patients are summarized in the Table. In all cases, the temporal lobes (superior, middle, and inferior temporal gyrus)

From the Department of Neurology (AH, TY, KS, YU), Fukushima Medical University, Fukushima; Departments of Neurology (MN) and Pathology (HT, AK), Brain Research Institute, University of Niigata, Niigata, Japan.
Send correspondence and reprint requests to: Akihiko Hoshi, MD, PhD, Department of Neurology, Fukushima Medical University, Fukushima 960-1295, Japan; E-mail: hoshia@fmu.ac.jp
This work was supported by a Collaborative Research Project Grant (2224) from the Brain Research Institute, University of Niigata, Niigata, Japan.
Supplemental digital content is available for this article. Direct URL citations appear in the printed text and are provided in the HTML and PDF versions of this article on the journal's Web site (www.jneuropath.com).

TABLE. Patient Clinical and Neuropathologic Data

Case	Sex	Age at Death, y	PMI, h	Braak Stage	Brain Weight, g	Aβ42 Deposit	Aβ40 Deposits
Control 1	M	76	3.5		1,270	1	0
Control 2	M	80	3		1,300	1–2	1
Control 3	F	82	4.5		1,210	1	1
Control 4	M	77	22		1,175	1–2	1
Control 5	M	76	2		1,275	1	0
sAD1	F	104	3.5	VI/C	780	3–4	2–3
sAD2	F	86	4.5	VI/C	860	3–4	1
sAD3	F	86	4	VI/C	995	4	2–3
sAD4	F	100	3	VI/C	935	3	1
sAD5	M	78	3.5	VI/C	910	3–4	1–2
fAD1	F	65	3.5	VI/C	750	4	1
fAD2	F	57	4	VI/C	470	4	2–3
fAD3	F	66	3	VI/C	910	4	1

Grading of Aβ 42 and 40 deposits: 0 = absent, 1 = few, 2 = moderate, 3 = many, 4 = very many.
sAD indicates sporadic Alzheimer disease; fAD, familial Alzheimer disease; fAD mutations: fAD1, fAD3, amyloid precursor protein (APP), 717ValIle; fAD2, presenilin L381V. M, male; F, female; PMI, postmortem interval.

were used for the immunohistochemical study. The extent of Aβ42 and Aβ40 deposition in immunostained sections was rated semiquantitatively, as previously reported (4).

Immunohistochemistry

Tissue samples were processed into 4-μm-thick paraffin-embedded sections, and immunostaining was performed using the EnVision (Dako, Glostrup, Denmark) system. The sections were deparaffinized, and nonspecific binding was blocked with 2.4% goat serum and 30% H_2O_2 for 30 minutes at room temperature. After washing with phosphate-buffered saline, the slides were incubated overnight at 4°C with primary antibodies. The primary antibodies and dilutions used were rabbit polyclonal anti-AQP1 antibody (1:1000; Chemicon International, Temecula, CA), rabbit polyclonal anti-AQP4 antibody (1:500; Santa Cruz Biotechnology, Santa Cruz, CA), rabbit polyclonal anti-Aβ42 antibody (1:500; Calbiochem, Billerica, MA), rabbit polyclonal anti-Aβ40 antibody (1:500; Calbiochem, Millipore), and mouse monoclonal anti–glial fibrillary acidic protein (GFAP) antibody (1:1000; Chemicon). For Aβ40 or Aβ42 immunostaining, sections were pretreated with 98% formic acid for 5 minutes. Subsequently, secondary antibody incubations were carried out for 45 minutes at room temperature. Peroxidase labeling was visualized using diaminobenzidine as a chromogen. For double staining, we used the EnVision G|2 double-stain system (Dako) in accordance with the manufacturer's protocol. Visualization was based on peroxidase using diaminobenzidine and alkaline phosphatase with permanent red as the chromogen.

Fluorescence immunohistochemistry was also performed on paraffin sections to characterize the relationship between the expression of AQP and that of Aβ. The primary antibodies and dilutions used were rabbit polyclonal anti-AQP1 antibody (1:1000), mouse monoclonal anti-Aβ42 antibody (1:300; Millipore), rabbit polyclonal anti-AQP4 antibody (1:500), and mouse monoclonal anti-Aβ40 antibody (1:25; Immuno-Biological Laboratories Co., Gunma, Japan). The secondary antibodies and dilutions used were fluorescein isothiocyanate–coupled goat anti-mouse IgG (1:100; KPL, Gaithersburg, MD), and Cy3-conjugated donkey anti-rabbit IgG (1:100; Jackson ImmunoResearch, West Grove, PA). Immunostained sections and fluorescent specimens were analyzed using a microscope digital camera system (DP70; Olympus, Tokyo, Japan).

Statistical Analysis

In all AD cases, the fluorescence intensity of AQP1 and Aβ42 was evaluated as relative fluorescence units and quantified using image analysis software (Lumina Vision; Mitani Corp., Tokyo, Japan), as reported previously (21). About 4 to 6 areas of 0.14 mm^2 were randomly selected from photographs of specimens that had been immunostained for AQP1 and Aβ42 taken from the superior, middle, and inferior temporal cortices of patients with AD. Correlations between AQP1 and Aβ42 levels in relative fluorescence units were assessed using both Spearman correlation and regression analyses. Statistical significance was set at $p < 0.05$. AQP1 or AQP4 immunoreactivity (IR) in the cerebral cortex was also semiquantified using image analysis software (Win Roof; Mitani Corp.), as described previously (25). The quantification measure, referred to as the relative density, was defined as the saturation value of AQP1 or AQP4 immunostaining on digitized images. Three random areas, each measuring 3.44 mm^2 in the superior, middle, and inferior temporal cortices, were assessed in all cases. All data were expressed as means ± SD. One-way ANOVA, followed by the Bonferroni test, was performed for statistical comparisons of the semiquantitatively measured AQP4 IR levels. Differences at $p < 0.05$ were regarded as statistically significant.

RESULTS

Aβ Deposition

All AD cases had numerous Aβ42 deposits in the cortex but the extent of Aβ40 accumulation relative to Aβ42 was highly variable (Table). Aβ40 deposits in both leptomeningeal and intracortical small vessels and capillaries were also

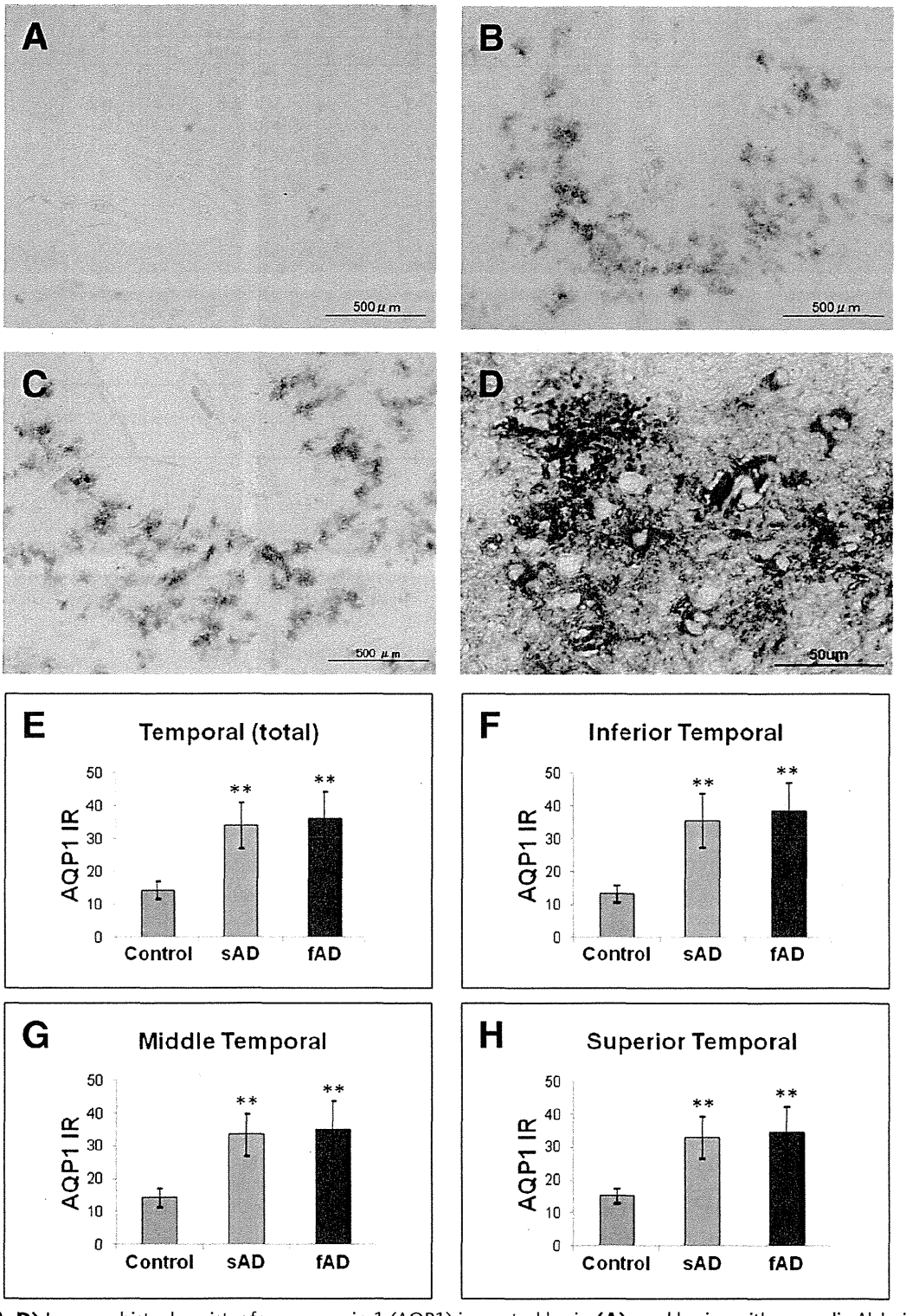

FIGURE 1. (A–D) Immunohistochemistry for aquaporin 1 (AQP1) in control brain **(A)**, and brains with sporadic Alzheimer disease (sAD) **(B)**, and familial Alzheimer disease (fAD) **(C)**. There are more numerous AQP1-positive cells in the cerebral cortex of both the sAD and fAD brains versus the controls. **(D)** Double immunolabeling of AQP1 (brown) and glial fibrillary acidic protein (GFAP) (red) in a case of AD. **(E–H)** The cortical levels of AQP1 immunoreactivity in both the sAD and fAD groups were significantly higher than in the control group. Data are given as mean ± SD. **, $p < 0.01$ versus control.

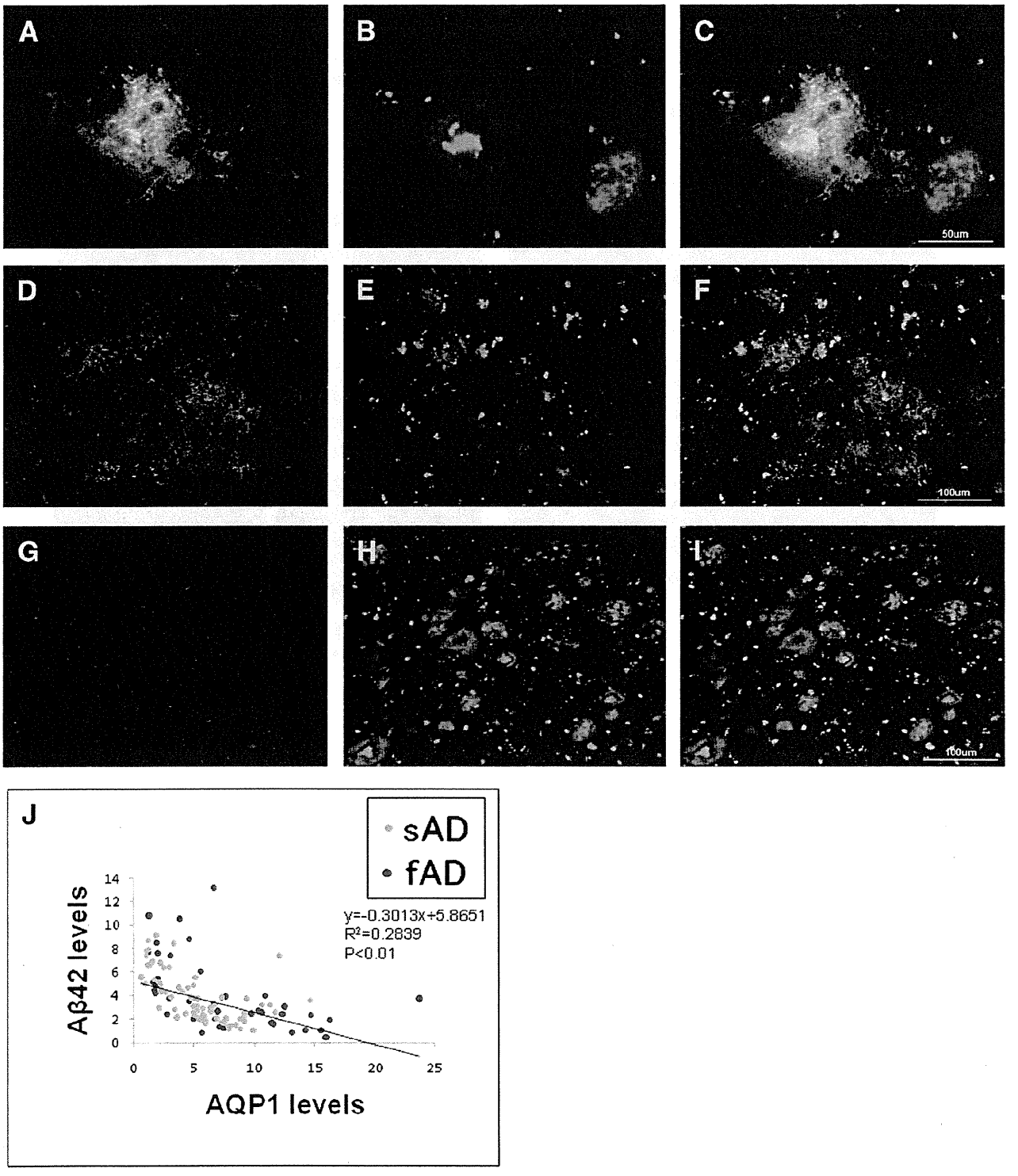

FIGURE 2. (A–I) Double immunofluorescence for aquaporin 1 (AQP1) **(A, D, G)** and amyloid-β peptide 1–42 (Aβ42) **(B, E, H)** in the Alzheimer disease (AD) groups **(C, F, I**: merged images**)**. Cells showing intense AQP1 expression are in contact with classic Aβ42 plaques **(A–C)**. Numerous AQP1-positive cells are present in areas where Aβ42 plaques are sparse **(D–F)**, but are not often observed in areas where such plaques are dense **(G–I)**. **(J)** Plot of Aβ42 levels and AQP1 levels (in relative fluorescence units) in the sporadic and familial AD groups. Semiquantitative analysis of AQP1/Aβ42 levels in both AD groups revealed a significant negative correlation between the cortical levels of AQP1 and that of Aβ42 ($R^2 = 0.2839$, $p < 0.01$).

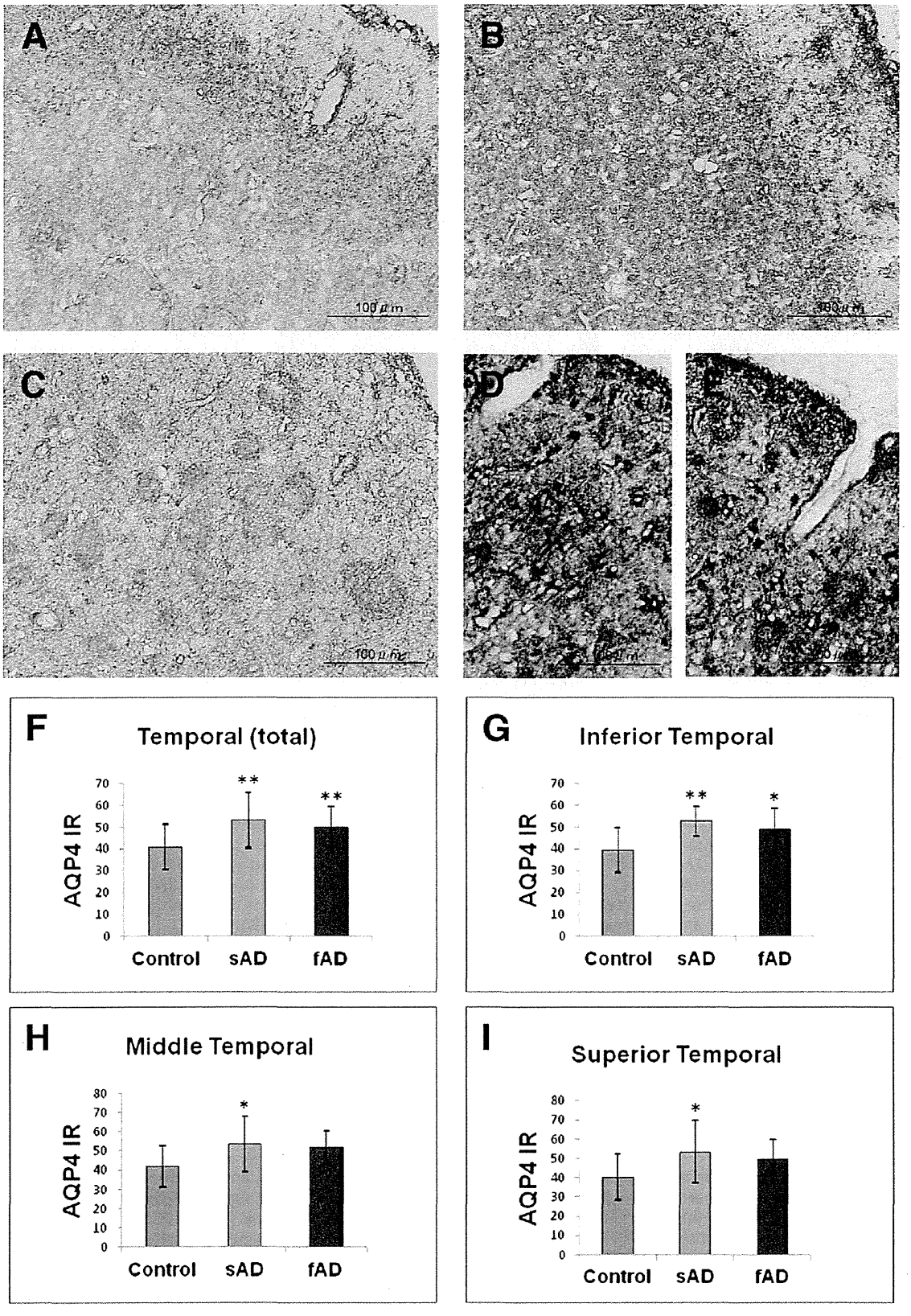

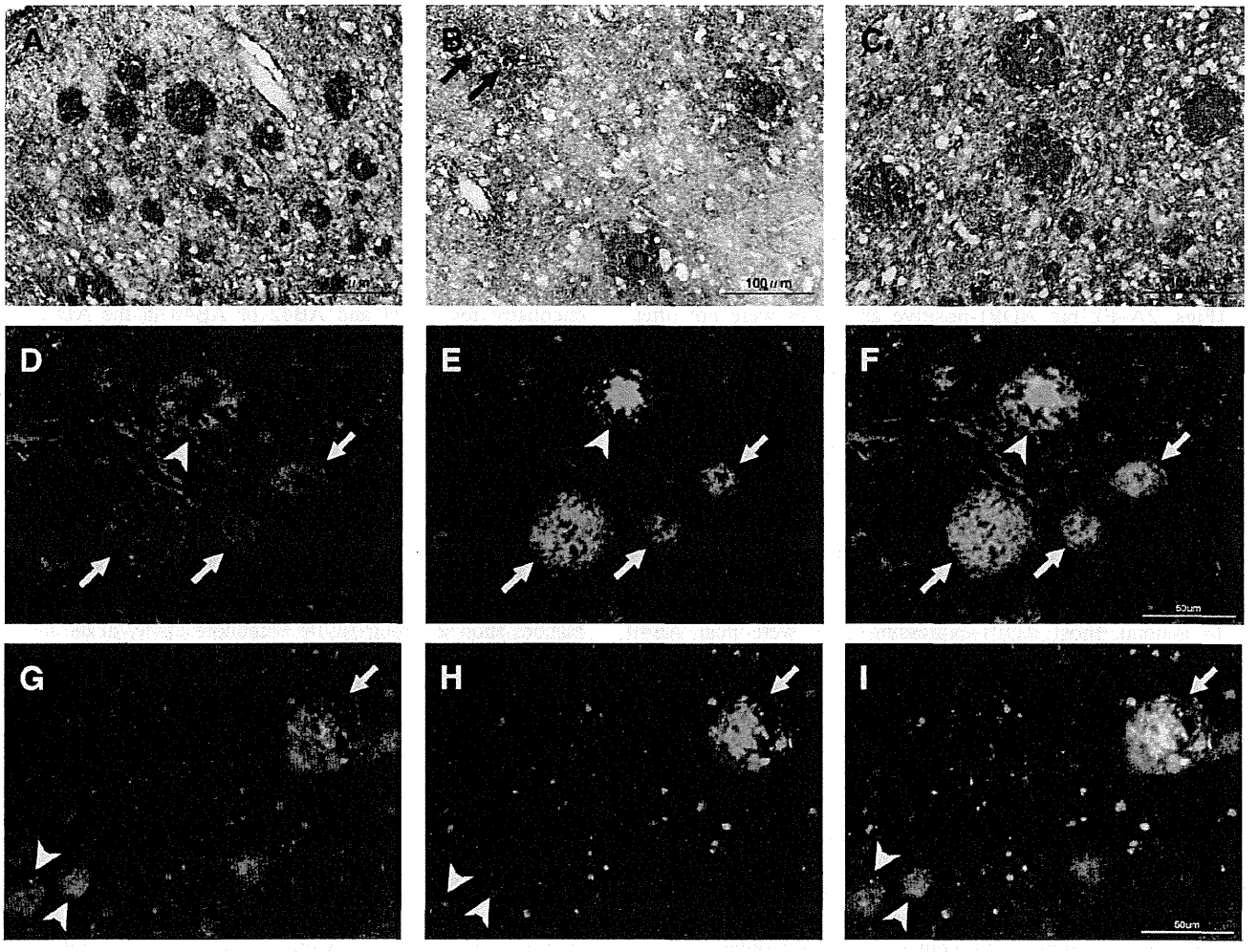

FIGURE 4. (A–C) Double-labeling immunohistochemistry for aquaporin 4 (AQP4) (brown) and amyloid-β peptide 1–42 (Aβ42) (red) **(A)** or amyloid-β peptide 1–40 (Aβ40) Aβ40 (red) **(B, C)** in cases of Alzheimer disease (AD). Numerous Aβ42 or Aβ40 plaques colocalize with intense Aβ plaque-like AQP4 expression **(A, C)**. There are smaller Aβ40-positive deposits within areas of plaque-like AQP4 expression **(B**, arrows**)**. **(D–I)** Double immunofluorescence for AQP4 **(D, G)** and Aβ42 **(E)** or Aβ40 **(H)** in the AD groups **(F, I**: AQP1/Aβ42 or Aβ40 merged images**)**. Classic Aβ42 plaques are devoid of AQP4 immunoreactivity in the dense core but show enhanced AQP4 expression at the margins **(D–F**, arrowheads**)**. AQP4 immunoreactivity is strong in the interior of primitive Aβ42 or Aβ40 plaques **(D–I**, arrows**)** or around areas of smaller Aβ40 deposits **(G–I**, arrowheads**)**.

observed in the patients with AD. Age-matched controls showed only a few or modest accumulations of Aβ42 deposits and no or only slight Aβ40 deposits (Table).

AQP1 Expression and Its Relationship to Aβ Deposition

AQP1-positive cells were more abundant in the cerebral cortex of both the sAD and fAD groups versus the controls (Figs. 1A–C). Numerous AQP1-positive cells in both AD groups were mainly in the pyramidal cell layers and had the morphologic characteristics of bushy reactive astrocytes, with hypertrophic cell bodies and highly branched processes. Double immunostaining for AQP1 and GFAP showed that these cells coexpressed both molecules (Fig. 1D). The levels of cortical AQP1 IR in both the sAD and fAD groups were significantly greater than in the control group. AQP1 IR in

FIGURE 3. (A–C) Immunohistochemistry for aquaporin 4 (AQP4) in a control brain **(A)**, and in cases of sporadic Alzheimer disease (sAD) **(B)**, and familial Alzheimer disease (fAD) **(C)**. High-power views show subpial or superficial cortical AQP4 immunostaining. **(D, E)** Double-labeling immunohistochemistry for AQP4 (brown) and glial fibrillary acidic protein (GFAP) (red) in the cortex of AD brains. AD brains showed intense AQP4 expression and GFAP-immunoreactive astrocytes **(D)** or marked Aβ plaque-like AQP4 expression **(E)**. **(F–I)** Cortical levels of AQP4 immunoreactivity in both the sAD and fAD groups are significantly greater than the in the control group, except for the middle and superior temporal cortices in the fAD group. Data are given as mean ± SD. **, $p < 0.01$ versus control; *, $p < 0.05$ versus control.

each case, expressed as the mean ± SD for the total, inferior, middle, and superior temporal cortices, was 14.2 ± 2.8, 13.2 ± 2.6, 14.2 ± 3.0, and 15.2 ± 2.4 in the control group; 34.0 ± 7.0, 35.4 ± 8.3, 33.5 ± 6.4, and 33.0 ± 6.5 in the sAD group; and 36.0 ± 8.4, 38.4 ± 8.7, 35.0 ± 8.71, and 34.5 ± 8.1 in the fAD group, respectively (Figs. 1E–H).

To confirm the observed relationship between the patterns of AQP1 and Aβ42 expression in AD, we next conducted a double immunofluorescence analysis of AQP1 and Aβ42 in all of the AD cases. AQP1-expressing cells were often localized near Aβ42 plaques in the sAD and fAD cases (Figs. 2A–F), but AQP1-positive astrocytes were not often observed in areas of densely packed Aβ42 plaques (Figs. 2G–I). There were numerous AQP1-positive cells in areas where Aβ42 plaques were sparse (Figs. 2D–F). There were significant negative correlations between the levels of AQP1 and Aβ42 expression when assessed semiquantitatively in the AD groups (Fig. 2J). Similarly, increased AQP1 IR was observed in areas where Aβ40 plaques were sparse (Figure, Supplemental Digital Content 1, Parts A and B, http://links.lww.com/NEN/A361), whereas expression was decreased in Aβ40-rich areas (Figure, Supplemental Digital Content 1, Parts C and D, http://links.lww.com/NEN/A361). In general, most AQP1-expressing cells were near Aβ40 plaques (Figure, Supplemental Digital Content 1, Parts E–G, http://links.lww.com/NEN/A361). Negative controls, in which incubation with anti-AQP1 antibody had been omitted, showed no IR (data not shown). The epithelial cells of the choroid plexus were intensely labeled with anti-AQP1 antibody (data not shown).

AQP4 Expression and Its Relationship to Aβ Deposition

Cortical AQP4 immunoreactivity was also more intense in both the sAD and fAD groups than in the control group (Figs. 3A–C; Figure, Supplemental Digital Content 2, Parts A–C, http://links.lww.com/NEN/A362). There were 2 prominent patterns of subpial or superficial cortical AQP4 immunoreactivity in the AD groups: intense diffuse AQP4 labeling of the entire neuropil (Fig. 3B) and AQP4 distribution around Aβ plaque-like bodies (Fig. 3C). The latter pattern was more apparent in fAD cases with an amyloid precursor protein mutation than in a case with a presenilin mutation (Table), but this was also seen in some patients with sAD. In the deeper cortical layers of control brains, there was less intense AQP4 immunoreactivity in cells with astrocyte morphology around vessels (Figure, Supplemental Digital Content 2, Part D, http://links.lww.com/NEN/A362). In the AD brains, intense AQP4 expression patterns that resembled astrocytic profiles (Figure, Supplemental Digital Content 2, Part E, http://links.lww.com/NEN/A362) or Aβ plaque-like AQP4 expression (Figure, Supplemental Digital Content 2, Part F, http://links.lww.com/NEN/A362) were observed in the deeper cortical layers. As shown in Figure 3, F to I, the cortical AQP4 IR in both the sAD and fAD groups was significantly greater than that in the control group, except for in the middle and superior temporal cortices in the fAD group. AQP4 IR in each case, expressed as the mean ± SD for the total, inferior, middle, and superior temporal cortices, was 40.9 ± 10.3, 39.3 ± 10.3, 41.7 ± 10.6, and 40.2 ± 12.0 in the control group; 53.1 ± 12.7, 52.6 ± 6.8, 53.4 ± 14.1, and 53.3 ± 16.3 in the sAD group; and 49.9 ± 9.2, 48.9 ± 9.2, 51.7 ± 8.9, and 49.3 ± 10.4 in the fAD group. Double labeling using both anti-AQP4 and anti-GFAP antibodies clearly showed that areas of AQP4 expression coincided with areas of GFAP expression in the cortex of the control group (data not shown). In contrast, AQP4 immunoreactivity was clearly observed in both astrocytosis and Aβ plaque-like structures in the AD groups (Figs. 3D, E).

We then conducted double-labeling immunohistochemistry for AQP4 and Aβ42 or Aβ40 in the AD cases. As expected, numerous Aβ42 or Aβ40 plaques were colocalized with intense expression of Aβ plaque-like AQP4 (Figs. 4A–C), and small Aβ40-positive deposits were detected within some areas of Aβ plaque-like AQP4 expression (Fig. 4B). To examine the expression patterns of AQP4 in both Aβ42 and Aβ40 plaques in detail, we conducted a double-immunofluorescence study of AQP4 and Aβ42 or Aβ40 in the AD groups. A noteworthy finding was that classic Aβ42 plaques were devoid of AQP4 immunoreactivity in the dense core, although AQP4 expression was enhanced at the marginal rim (Figs. 4D–F, arrowheads). Primitive Aβ42 or Aβ40 plaques showed strong AQP4 immunoreactivity in the interior (Figs. 4D–I, arrows) or around areas of light Aβ deposition (Figs. 4G–I, arrowheads).

Lastly, we investigated the expression of AQP4 around Aβ40-positive vessels, that is, larger vessels and capillaries with CAA. Intriguingly, various degrees of AQP4 expression were noted around Aβ40-positive vessels (Figs. 5B–F). Intense AQP4 immunoreactivity was observed around larger vessels showing slight to moderate Aβ40 positivity (Figs. 5B, C) in comparison to that around Aβ40-negative vessels (Fig. 5A). Loose AQP4 reaction products with irregular perivascular spaces distributed around larger vessels with intense Aβ40 positivity were also observed, in contrast to Aβ40 plaques associated with massively enhanced AQP4 expression (Fig. 5D). In addition, AQP4 expression around capillaries with CAA tended to be more intense with dyshoric changes, that is, Aβ40 spreading into the neuropil (Figs. 5E, F).

DISCUSSION

The marked variation of AQP expression in AD brains observed in the present study raises the possibility that AQP1-positive reactive astrocytes may pathologically modify the deposition of Aβ and that Aβ deposits may alter the astrocytic expression of AQP4 during the development of AD. In both the sAD and fAD groups, many AQP1-positive reactive astrocytes were close to deposits of Aβ42 or Aβ40, whereas AQP1 immunoreactivity in astrocytes was often reduced in areas of intense Aβ immunoreactivity, suggesting that AQP1 expression is associated with transition to an Aβ42- or Aβ40-rich state. Other noteworthy features included the presence of intense Aβ plaque-like AQP4 expression associated with Aβ42- or Aβ40-positive SPs and various degrees of AQP4 expression around Aβ40-positive vessels. There were no apparent differences in AQP1 expression between the sAD and fAD groups, although fAD cases with amyloid

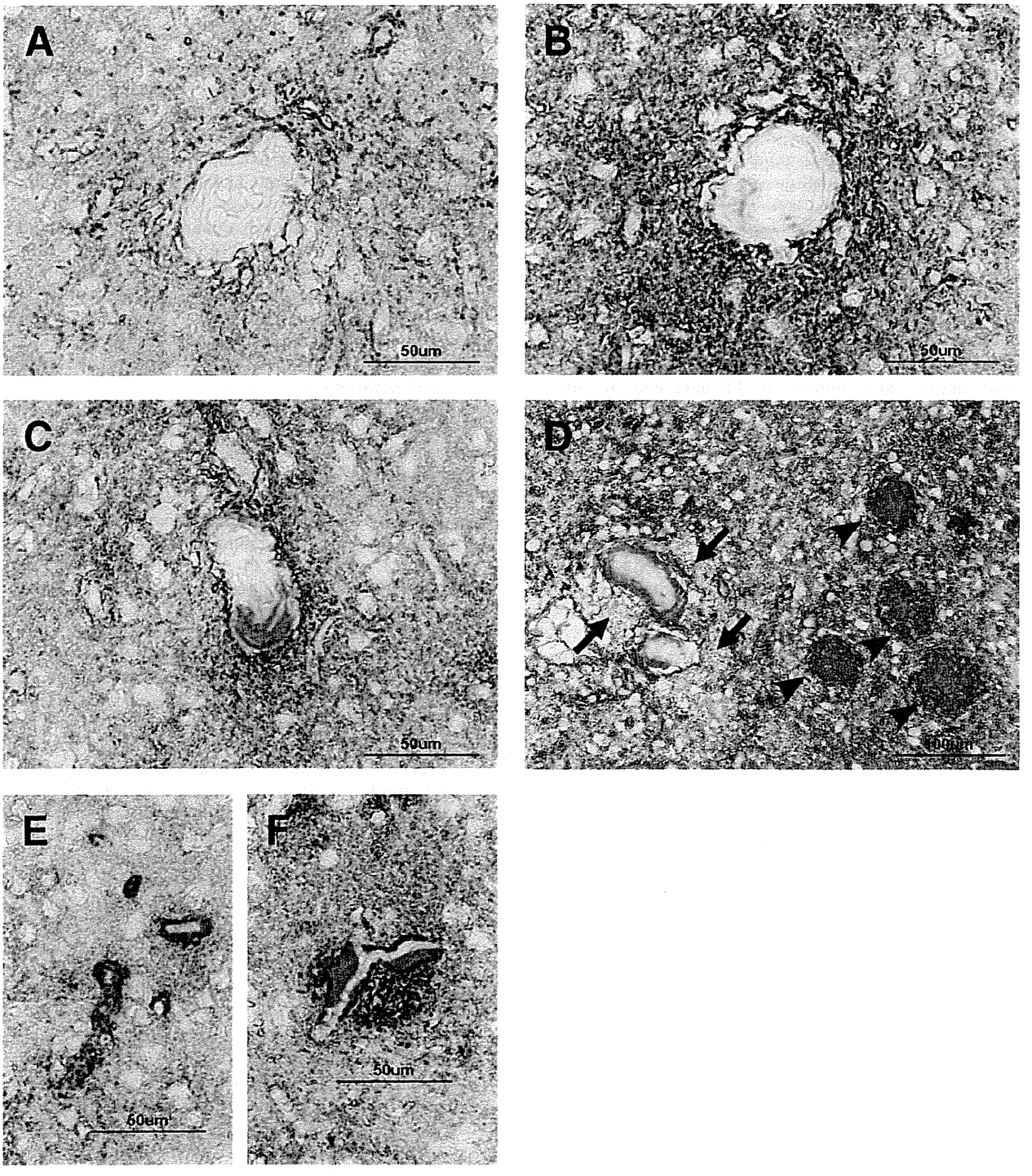

FIGURE 5. (A–F) Double-labeling immunohistochemistry for aquaporin 4 (AQP4) (brown) and amyloid β peptide 1–40 (Aβ40, red) in the Alzheimer disease (AD) groups with moderate or extensive Aβ40 deposits. Note the location of AQP4 expression around Aβ40-positive vessels. Strong AQP4 immunoreactivity is evident around slightly Aβ40-positive larger vessels **(B)** or moderately Aβ40-positive larger vessels **(C)** in comparison to the immunoreactivity around Aβ40-negative vessels **(A)**. **(D)** Loose fibrous expression of AQP4 around intensely Aβ40-positive larger vessels (arrows) and intense expression of AQP4 around areas with a high Aβ40 plaque burden (arrowheads). **(E, F)** AQP4 expression around cerebral amyloid angiopathy (CAA). Mild expression of AQP4 around capillary CAA showing slight or absent dyshoric change **(E)**. Intense expression of AQP4 around capillary CAA with dyshoric change **(F)**.